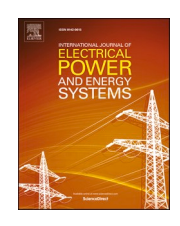


Contents lists available at ScienceDirect

International Journal of Electrical Power and Energy Systems

journal homepage: www.elsevier.com/locate/ijepes





Reactive power limit of wind farm with doubly-fed induction generators and its asymmetric P-Q dependence

Shenghu Li

School of Electrical Engineering and Automation, Hefei University of Technology, Hefei 230009, China

ARTICLE INFO

Keywords: Wind farm Reactive power limit Alternative solution P-Q dependence

ABSTRACT

The existing reactive power limit models of doubly-fed induction generators ignore the relation among wind speed, rotor speed, and active power output. Furthermore, they are decided by stator voltage and reactive power setting, but the former is uncontrollable, and the latter is different from the maximum/minimum reactive power. The reactive power limit of wind farm with doubly-fed induction generators and collectors is important to power system dispatch, but has not been studied. In this paper, iterative solution to reactive power limit model of the doubly-fed induction generator is proposed, with the novelty of correspondence of wind speed to active power, not using simplified slip power, and independent of the reactive power setting. By alternatively solving the reactive power limits of the doubly-fed induction generators and power flow of the collectors, the reactive power limit of wind farm is proposed, which is based on the voltage at the point of common coupling instead of the stator voltage. It is found that with the same wind speed and grid voltage, the upper/lower reactive power limit of wind farm is asymmetrical. Dependence of active power on the reactive power limit is newly described by a quadric function. Simulation results give the reactive power limit of the doubly-fed induction generators and wind farm, compare the active power at the upper/lower reactive power limit, and verify the impacts of the voltage at the point of common coupling and wind speed on the dependence of active power on the reactive power limit.

1. Introduction

Due to fuel energy depletion and environment concern, the renewable powers, mainly hydro power, wind power, and photovoltaic, increase quickly in recent years. The European countries, e.g. Denmark, Irish, UK, and Spanish, are the pioneer of wind power utilization, followed by many other counties. In Europe, the roadmap 2050 to emission-free power system relies on the renewables. In China, the electric power generation from wind and solar power in 2004 accounts for about 18 % of the total electricity consumption.

With the increasing wind power, the wind turbine generators (WTGs), e.g. the doubly-fed induction generators (DFIGs) and permanent-magnet synchronous generators, gradually displace the thermal synchronous generators (SGs), which requires the WTGs to operate as the SGs, participating into system dispatch, frequency regulation, transient stability[1], damping control [2,3], etc.

1.1. Research Motivation and difficulty

The active power dispatch keeps power balance and system frequency. For comparison, the reactive power is less focused but critical to ride-through fault [4], maintain voltage level [5,6], adjust power flow, and reduce power loss [7]. In many studies, the reactive power of the DFIG is fixed or proportional to the active power [8,9]. The reactive power limit (RPL), i.e. the maximum/minimum reactive power, is ignored, hence the adjustability of the DFIG is not fully utilized.

The DFIG's RPL is decided by the limits of the stator, the rotor, and grid-side converter (GSC). For the dynamic control, the limit is set by currents instead of reactive power. The difficulty is how to set the limit of the dq current components for the decoupled power control [10]. However, the dynamic control is in the time scale of seconds or ms, which may yield the RPL more optimistic than that in long-term, e.g. steady-state, operation.

For steady-state analysis, the difficulties to quantify the RPL of the wind farm lie in,

Abbreviations: DFIG, Doubly-fed induction generator.; MPPT, Maximum power point tracking.; PCC, Point of common coupling.; Re, Im, Real and imaginary parts.; RPL, Reactive power limit.; RSC, GSC, Rotor-side and grid-side converters.; Set, Parameter setting.; SG, L, Synchronous generator, load.; WF, C, Wind farm, collector.; WT, WTG, Wind turbine, wind turbine generator..

Nomenclature

A, λ , β , s Sweep area, tip-speed ratio, pitch angle, slip.

 C_p Power utilization coefficient of the WT.

 λ_i Intermediate parameter of the WT.

 c_1 - c_9 Parameters in C_p function of the WT.

 ρ , $v_{\rm w}$ Air density, wind speed.

R, *X* Resistance, reactance.

G, **B** Conductance matrix, susceptance matrix.

 \overline{I} , I Current phasor and its magnitude.

 $\overline{V} = V \angle \theta$ Voltage phasor, its magnitude and angle.

P, *Q* Active and reactive powers.

J Jacobian matrix.

 μ Index to show error of simplified slip power.

 ξ_1 , ξ_2 Indices to show different P_{WF} at the RPL.

 a_0 , a_1 , a_2 Coefficients of the quadric function.

 γ , ε Radius, convergence criterion.

Subscripts

m, em Magnetizing circuit, electromagnetic.

M Mechanical parameter. s, r, g Stator, rotor (or RSC), GSC.

- (1) Inexact relation among the RPL, the wind speed, the slip, and the DFIG's output. The RPL given in [11] ignores the GSC. Consequently, the RPL of the DFIG is pessimistic since the GSC may also produce or absorb the reactive power. Furthermore, the active slip power through the converters is ignored, hence the active power output of the DFIG is inexact. The RPL is defined by the maximum capacity of the stator and GSC in [12,13], but active powers at the stator and the converters are calculated independently, i.e. the relation of the active slip power with the active stator power is not considered. Seeing that the relation of the converters' active power (slip power) with the stator power is decided by the slip, the DFIG's RPL with active power is proposed by Lund and Engelhardt [14,15], and applied in many literatures [16–19]. But this model is also not accurate due to simplified modeling to the DFIG,
- (a) Definition to slip power ignores the windings resistances. Different from those of the SG, the voltage and current of the DFIG are low and the windings resistances are large. Ignoring the resistance will misjudge active power and yield inaccurate RPL of the DFIG.
- (b) The curve of the RPL vs. active power is drawn for one slip. But actually one wind speed only has an optimal slip and a captured power only, i.e. the RPL based on one slip is not a curve, otherwise the active power is inconsistent with the slip and the wind speed.

Hence the detailed solution to the DFIG is applied in [20] to derive the windings' currents and the DFIG's RPL under the maximum power point tracking and the derated mode respectively. It seems to be perfect, but still has error and drawback,

- (a) Solution to the DFIG is based on initial reactive power, but the latter is not equal to the maximum/minimum reactive power limits of the DFIG. In other words, different initial reactive power settings will yield different RPLs, which is obviously wrong.
- (b) Solution is based on given stator voltage of the DFIG. But the stator voltage is not fixed due to change of the wind speed and the voltage at the point of common coupling (PCC). Hence the existing RPL model of the DFIG has little value to the power system dispatchers.

- (2) There is no exact RPL model of wind farm for power system dispatch. Due to small capacity and numerous units of the DFIGs, the RPL of wind farm is more useful to the system operator than that of the DFIG [21]. But the existing dispatch studies to the wind farm either casually set the reactive power limit of the DFIG, or assume the RPL of the wind farm is that of the DFIG multiplied by the number of the DFIGs, which is wrong considering power loss of collectors and transformers. For example in [22], the RPL of the DFIG is assumed to be fixed, thus the tape changer is used to extend the RPL of wind farm [23]. The Q-V curve of the collectors is got from power flow equations for voltage control [24,25], but the unified solution to the RPL of wind farm with the DFIGs and the collectors has not been found yet. The reason is not only the difficulty of deriving DFIG's RPL, but also convergence due to obviously different impedances and R/X ratios of the DFIGs and collectors. It's difficult to solve the DFIG's RPL and the power flow of the collectors together.
- (3) Dependence of active power on the RPL is not found. If the RPLs of the DFIGs and wind farm are available, there is another problem. As seen in this paper, due to the power loss of the windings, the collectors, and/or the transformers, the upper/lower RPL of wind farm (or the DFIGs) is not symmetrical. Thus even the PCC voltage is fixed, the same wind speed yields 2 active powers. Such dependence is negligible for the SG with small resistance, but obvious for the wind farm where the DFIGs have low voltage, small capacity, and relative large active power loss, which has not been studied yet.

Investigation to the RPL models of the DFIG and the wind farm is summarized in Table 1.

Therefore the challenge to derive the RPL of the wind farm with the DFIGs and the collectors lies in,

- (a) How to derive the exact RPL model of the DFIG. The existing RPL curve is based on a given slip and the slip power ignores windings' resistances, thus can not give exact relation of the RPL to the wind speed, the slip, and the active power. Furthermore, the solution is based on the initial reactive power of the DFIG, which is not consistent with the resultant RPL.
- (b) How to derive the RPL of wind farm. Due to the power loss of the collectors, the RPL of wind farm is not the sum of those of the DFIGs. It's difficult to solve the DFIGs' RPLs and the power flow

Table 1Investigation to the RPL of DFIG and wind farm.

RPL modeling	Comments	Sources
RPL of DFIG based on stator power constrained by stator current limit, similar to that of the SG.	Ignore the power from the RSC and GSC, power loss of DFIG is inaccurate, and can not differentiate active powers of WT and DFIG.	Most papers
RPL of DFIG based on stator power constrained by stator current limit and rotor current limit, plus the GSC power constrained by GSC current limit.	Slip power not exactly defined, no relation among wind speed, rotor speed and output of DFIG, and can not differentiate outputs of WT and DFIG.	
RPL of DFIG with its C_p function and detailed solution to its inner constraint.	Based on given reactive power of DFIG, inconsistent with RPL, stator voltage uncontrollable.	Ref. [20]
RPL of DFIG with its C_p function and detailed solution to its inner constraint, independent of its reactive power setting.	Unavailable.	This paper
RPL of wind farm independent of reactive power settings of DFIGs and dependent on the PCC voltage.	Unavailable.	

- of the collectors together. Moreover, when solving the RPL of the DFIGs, the stator voltages are not fixed, but decided by the PCC voltage and the output of other DFIGs, which adds the difficulty to solve the RPL of the wind farm.
- (c) How to quantify dependence of active power of wind farm on its RPL. Since the latter is not symmetrical as proved in the paper, the active powers at the upper/lower RPL are not the same, even though wind speeds and PCC voltage do not change. There is no existing study quantifying the difference of the active powers or describing the dependence of the active powers on the RPL of the wind farm.

1.2. Contributions of this paper

- (a) The RPL of the DFIG independent of its reactive power is proposed. Compared with existing models, detailed power and torque constraints are included to solve the DFIG from the initial reactive power of the DFIG, but with iterative solution, the RPL is not dependent on initial reactive power, thus shows exact relation of wind speed, slip, active power, and the RPL. The slip power which ignores the resistances of the windings is not used to derive the RPL of the DFIG.
- (b) The RPL model of wind farm related to the PCC voltage is newly proposed. With the DFIGs operating at the RPL, the power flow of the collectors is solved repeatedly to decide the stator voltages and update the RPLs of the DFIGs. The final reactive power at the PCC is the RPL of wind farm. With the alternative solution, it does not require the stator voltages to be fixed, or the wind speeds to be identical.
- (c) It is newly found that the upper/lower RPL of wind farm are not symmetrical. So even though the wind speeds and PCC voltage do not change, the active powers of wind farm at the upper/lower RPL are different, as evaluated with two indices. The dependence of active power of wind farm on its reactive power is newly described by a quadric function. Impact of the PCC voltage and wind speeds on this dependence is quantified.

1.3. Paper Organization

The paper is organized as follows. In Section II, the existing RPL model of the DFIG is discussed to show the drawback. In Section III, the improved DFIG's RPL model considering the windings' resistance and independent of initial reactive power setting is proposed. In Section IV, the RPL of wind farm with the stator voltages decided by the PCC voltage is proposed. It is newly found that the upper and the lower RPL correspond to two active powers of wind farm, then data fitting technique is applied to describe the relation of the active/reactive powers at the RPL. In Section V, the simulation results are provided to verify the feasibility and accuracy of proposed RPL models. In Section VI, conclusions are given.

2. Existing reactive power limit model OF DFIG

The factors related to the RPLs of the DFIG and wind farm (WF) are shown in Fig. 1. The DFIG's RPL is decided by wind speed $v_{\rm w}$, the slip s, the stator voltage $V_{\rm s}$, reactive power of the DFIG and GSC, i.e. $Q_{\rm DFIG,set}$.

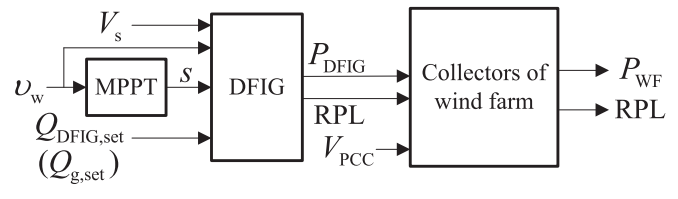


Fig. 1. The relative factors to the RPLs of DFIG and wind farm.

and $Q_{\rm g,set}$. The RPL of the wind farm is decided by active powers of the DFIGs, i.e. $P_{\rm DFIG}$, the RPLs of the DFIGs, and the PCC voltage, i.e. $V_{\rm PCC}$.

As shown in Fig. 2(a), a DFIG has the wind turbine (WT), the transfer shaft, the induction generator, the rotor-side converter (RSC), and the GSC, where $\overline{V} = V \angle \theta$ is the voltage, \overline{I} and I is current and its magnitude, R is the resistance, X is reactance, s is the slip, the subscripts s, r, and m denote the stator, the rotor, the magnetizing circuit respectively, and s, g denotes current or power flowing from the stator to GSC. With V_s and θ_s known, there are 6 variables to be solved, i.e. θ_m , V_m , θ_r , V_r , θ_g , and V_g . Based on Fig. 2 (b), the stator current and the equivalent rotor current are almost the same, with little error due to magnetization circuit. So their current limits of the stator and the rotor in the equivalent circuit are not obviously different. However, the rotor current limit is decided by not only the rotor winding but also the RSC. Usually the RSC is selected not restricting the capacity of the rotor winding. Similarly, the GSC is selected not restricting the capacity of the filter between the GSC and the stator.

With the stator current defined in (1), square of I_s is given in (2), constrained by the stator current limit $I_{s,max}$.

$$\overline{I}_{s,m} = \frac{\overline{V}_s - \overline{V}_m}{R_s + jX_s} \tag{1}$$

$$I_{s}^{2} = \frac{V_{s}^{2} + V_{m}^{2} - 2V_{s}V_{m}\cos\theta_{s,m}}{R_{s}^{2} + X_{s}^{2}} \leq I_{s,max}^{2}$$
 (2)

The stator power constrained by $I_{s,max}$ is given in (3), where P is the active power, Q is the reactive power, and γ is the radius.

$$(-P_{s,m})^{2} + (-Q_{s,m})^{2} \leqslant V_{s}^{2} I_{s,max}^{2} = \gamma_{s}^{2}$$
(3)

The stator voltage may be defined by the stator current and the rotor current.

$$\overline{V}_{s} = (R_{s} + jX_{s} + jX_{m})\overline{I}_{s} + jX_{m}\overline{I}_{r}$$

$$\tag{4}$$

With the stator current given by the stator power (5), the rotor current is given in (6).

$$\bar{I}_{s} = \frac{P_{s,m} - jQ_{s,m}}{\overline{V}_{s}^{*}} \tag{5}$$

$$\bar{I}_{\rm r} = \frac{V_{\rm s}^2 - [R_{\rm s} + j(X_{\rm s} + X_{\rm m})] (P_{\rm s,m} - jQ_{\rm s,m})}{jX_{\rm m} \bar{V}_{\rm s}^*}$$
(6)

Within the rotor current limit $I_{r,max}$ (7), the stator power constrained by the rotor current is given in (8) [20]. It is clear that the feasible region of the stator power is decided by the intersection of (3) and (8).

$$I_{m,r}^2 \leqslant I_{r,max}^2 \tag{7}$$

$$\left[-P_{s,m} + \frac{R_s V_s^2}{R_s^2 + (X_s + X_m)^2} \right]^2 + \left[-Q_{s,m} + \frac{(X_s + X_m) V_s^2}{R_s^2 + (X_s + X_m)^2} \right]^2 \leqslant \frac{X_m^2 V_s^2 I_{r,max}^2}{R_s^2 + (X_s + X_m)^2} \\
= \gamma_r^2 \tag{8}$$

With the GSC current limit $I_{g,max}$, the operation region of the GSC power is given by,

$$P_{s,g}^{2} + Q_{s,g}^{2} \approx s^{2} P_{s,m}^{2} + Q_{g,s}^{2} \leqslant V_{s}^{2} I_{g,max}^{2} = \gamma_{g}^{2}$$
(9)

The reactive power of the DFIG is the sum of those from the stator and the GSC (10), hence the operation region of the DFIG is the union of those of the stator and GSC, i.e. decided by (3), (8), and (9). The drawback of this RPL model is that it not related to the slip or the wind speed, thus has little application value.

$$Q_{\rm DFIG} = -Q_{\rm s,m} - Q_{\rm s,g} \tag{10}$$

By ignoring the windings resistance, the slip power is given by $P_{\rm g,s} =$

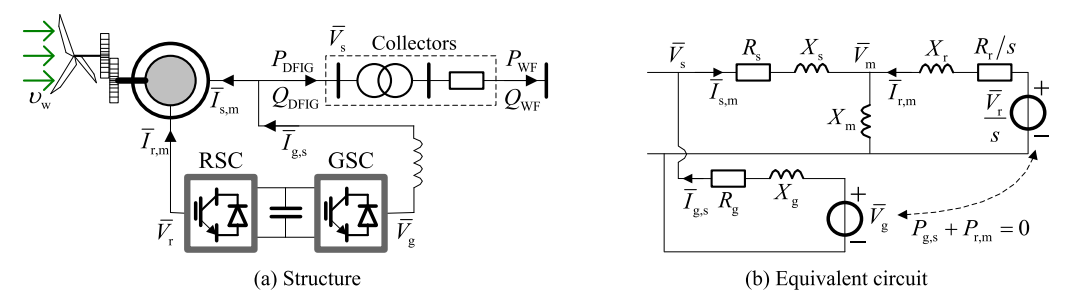


Fig. 2. Configuration and equivalent circuit of the DFIG.

 $-P_{r,m} \approx sP_{s,m}$. The active power output of the DFIG is given in (11), then P_{sm} and P_{sg} are given by P_{DFIG} (12).

$$P_{\rm DFIG} = -P_{\rm s,g} - P_{\rm s,m} \approx (1-s)(-P_{\rm s,m})$$
 (11)

$$\begin{cases}
-P_{s,m} \approx \frac{P_{DFIG}}{1-s} \\
-P_{s,g} \approx \frac{-sP_{DFIG}}{1-s}
\end{cases}$$
(12)

The operation region of the DFIG is decided by (13)-(15)[14,15,20]. With s = 0.25, they are 3 circles as shown in Fig. 3(a). With the intersection of (13) and (14), then with the union of (15), the resultant RPL of the DFIG is shown in Fig. 3 (b).

$$\left(\frac{P_{\text{DFIG}}}{1-s}\right)^2 + \left(-Q_{\text{s,m}}\right)^2 \leqslant r_{\text{s}}^2 \tag{13}$$

$$-\sqrt{r_{\rm s}^2 - \left(\frac{P_{\rm DFIG}}{1 - s}\right)^2} \leq Q_{\rm DFIG} + \frac{V_{\rm s}^2}{X_{\rm s} + X_{\rm m}} \leq \sqrt{r_{\rm r}^2 - \left(\frac{P_{\rm DFIG}}{1 - s}\right)^2}$$
(14)

$$\frac{s^2 P_{\rm DFIG}^2}{(1-s)^2} + Q_{\rm g,s}^2 \leqslant \gamma_{\rm g}^2 \tag{15}$$

The existing RPL model of the DFIG seems to be perfect, but it has the following errors,

- (a) It can not give exact correspondence of $v_{\rm W}$ to $P_{\rm DFIG}$. One may assume the captured power by the WT, i.e. $P_{\rm WT}$, is $P_{\rm DFIG}$. But considering the windings' loss, $P_{\rm WT} > P_{\rm DFIG}$, as shown with dotted lines in Fig. 3 (b), thus $P_{\rm DFIG}$ will be overestimated, and the RPL will be underestimated.
- (b) The simplified slip power ignores wingdings' resistance, i.e. assuming μ in (16) to be 0. But different from the SG, the DFIG has low voltage and large resistance, thus ignoring its resistances reduces the accuracy of the RPL.

$$\mu = -\frac{P_{\rm r,m}}{\rm s} - P_{\rm em} \tag{16}$$

(c) More importantly, the above RPL model is based on s, but s changes with $v_{\rm w}$ then decides $P_{\rm DFIG}$, thus is not fixed for different $P_{\rm DFIG}$. For example, with s= -0.05, the RPL is shown in Fig. 4, quite different from Fig. 3(b). Actually neither Fig. 3(b) nor Fig. 4 is correct, since s= -0.05 corresponds to $v_{\rm w}=8.65$ m/s, and $P_{\rm WDFIG}=0.306$ p.u. The RPL corresponding to s= -0.05 is only 2 points signed with 0 in Fig. 4. Other part of the curve is wrong.

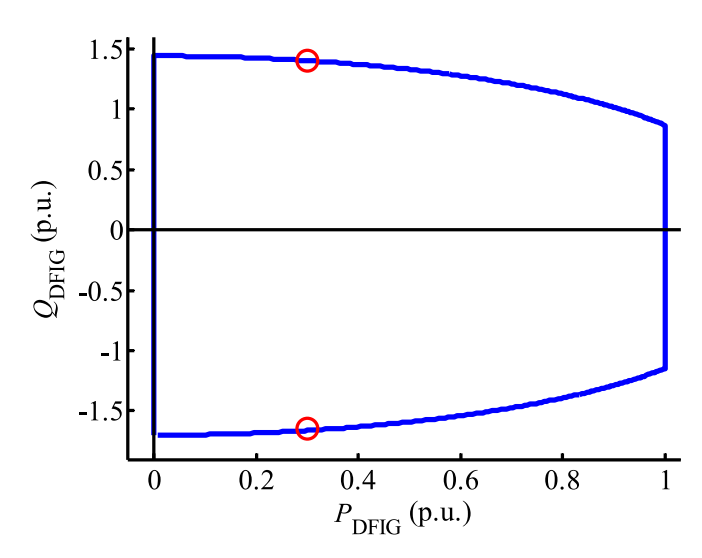
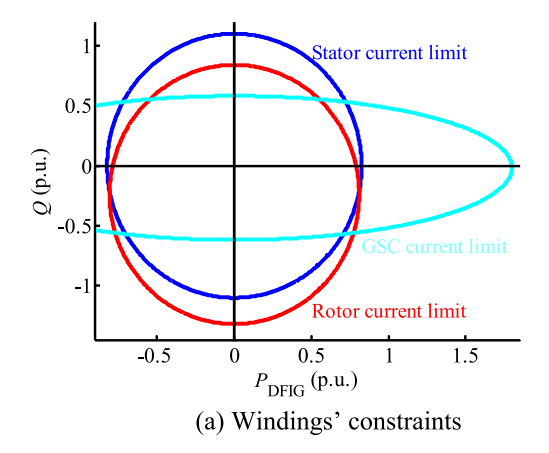


Fig. 4. Error of the existing RPL of DFIG with s = -0.05.



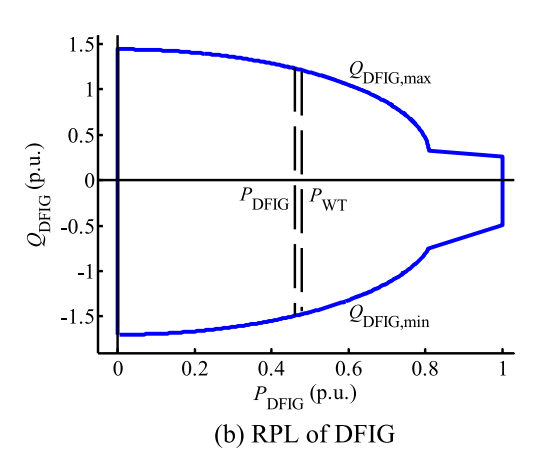


Fig. 3. Existing RPL of DFIG (s = 0.25).

3. Exact RPL model of DFIG

Most of the existing RPL models of the DFIG ignore the windings' resistance, and assume the captured power of the wind turbine equal to the active power of the DFIG. All of these models are decided by the setting to the reactive power and the stator voltage of the DFIG. However, the reactive power setting is different from the RPL of the DFIG, hence the RPL is inaccurate. The stator voltages of the DFIGs are not fixed or controllable due to wind speed change and system dispatch. The PCC voltage is controllable, thus the RPL of the wind farm with the DFIGs and the collectors are more valuable for system dispatchers, but detailed solution to the wind farm is seldom studied.

To bridge the above gap, in the following, the RPL model of the DFIG is improved, and the RPL model of wind farm is proposed, as shown in Fig. 5. Besides the Newton iterations to solve the DFIG and the collectors, there are 2 alternative solutions to update reactive power and stator voltage of the DFIGs in wind farm.

3.1. RPL of DFIG with detailed solution

To find the exact RPL of the DFIG, detailed solution to the DFIG is needed. Under the maximum power tracking (MPPT) mode, P_{WT} is given by (17)-(19), where ρ is the air density, A is the sweep area, C_p is the power utilization coefficient, β is the pitch angle, λ_i is an intermediate parameter, λ is the tip-speed ratio, and c_1 - c_9 are coefficients of C_p .

$$P_{\rm WT} = \frac{1}{2} \rho A C_p v_{\rm w}^3 \tag{17}$$

$$C_p = c_1 \left(\frac{c_2}{\lambda_i} - c_3 \beta - c_4 \beta^{c_5} - c_6 \right) e^{-\frac{c_7}{\lambda_i}}$$
 (18)

$$\frac{1}{\lambda_i} = \frac{1}{\lambda + c_8 \beta} - \frac{c_9}{\beta^3 + 1} \tag{19}$$

For a $v_{\rm W}$, by continually changing the rotor speed $\omega_{\rm WT}$ and comparing $P_{\rm WT}$, the maximum $P_{\rm WT}$, i.e. $P_{\rm WT,max}$, will be found, as seen in Fig. 6. The optimal rotor speed $\omega_{\rm WT,op}$ is also found.

The torque balance of the transfer shaft is given in (20), where Re denotes the real part, Δ denotes the increment, the subscript M denotes the mechanical parameter, and superscript * denotes the conjugate operation.

$$\Delta P_{\rm M} = -\frac{P_{\rm WT}}{1-s} + P_{\rm m,s} = -\frac{P_{\rm WT}}{1-s} + {\rm Re} \Big(\overline{V}_{\rm m} \overline{I}_{\rm m,s}^* \Big) \tag{20}$$

 Q_{DFIG} is not decided by v_{w} and may be set directly, hence its constraint is given in (21), where Im denotes the imaginary part, and the subscript set denotes the setting value. Since active power loss of the DFIG is unknown before solving the DFIG, P_{DFIG} can not be set, and the active power balance at the stator is not a valid constraint.

$$\Delta Q_{\rm s} = -Q_{\rm s,m} - Q_{\rm s,g} - Q_{\rm DFIG,set} = -\operatorname{Im}(\overline{V}_{\rm s}\overline{I}_{\rm s,m}^*) - \operatorname{Im}(\overline{V}_{\rm s}\overline{I}_{\rm s,g}^*) - Q_{\rm DFIG,set} \tag{21}$$

The active and reactive power balances of the magnetizing circuit are given by,

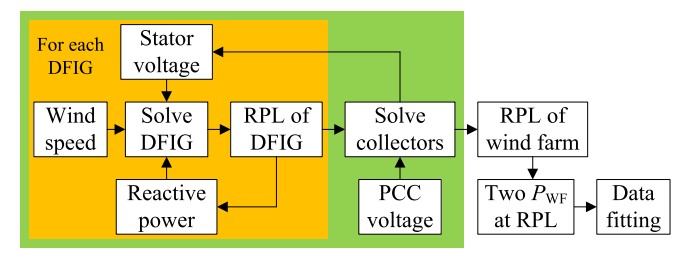


Fig. 5. Procedure to solve RPLs of DFIG and wind farm.

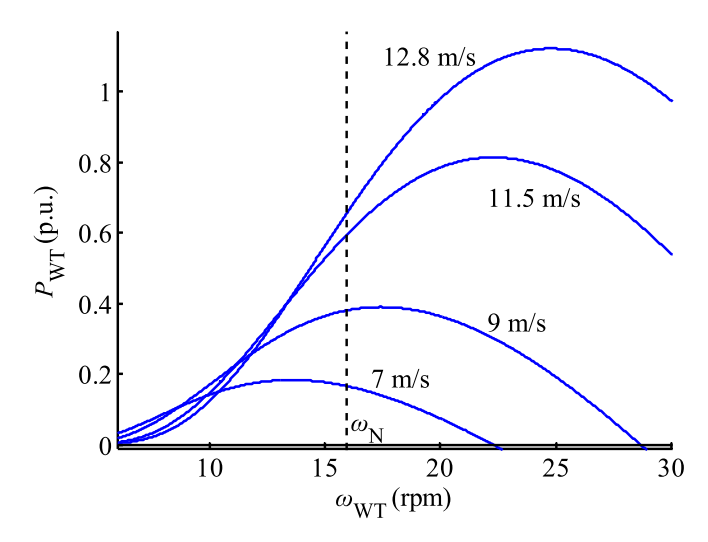


Fig. 6. Captured power of WT with different speeds.

$$\Delta P_{\rm m} = -P_{\rm m,s} - P_{\rm m,r} = -\operatorname{Re}\left(\overline{V}_{\rm m}\overline{I}_{\rm m,s}^{*}\right) - \operatorname{Re}\left(\overline{V}_{\rm m}\overline{I}_{\rm m,r}^{*}\right)$$
(22)

$$\Delta Q_{\rm m} = -Q_{\rm m,s} - Q_{\rm m,m} - Q_{\rm m,r} = -\operatorname{Im}\left(\overline{V}_{\rm m}\overline{I}_{\rm m,s}^{*}\right) - \frac{V_{\rm m}^{2}}{X_{\rm m}} - \operatorname{Im}\left(\overline{V}_{\rm m}\overline{I}_{\rm m,r}^{*}\right) \quad \ (23)$$

The active and the reactive power balances of the GSC are given by,

$$\Delta P_{g} = -P_{r,m} - P_{g,s} = -\operatorname{Re}\left(\overline{V}_{r}\overline{I}_{r,m}^{*}\right) - \operatorname{Re}\left(\overline{V}_{g}\overline{I}_{g,s}^{*}\right)$$
(24)

$$\Delta Q_{g} = Q_{s,g} + Q_{g,set} = \operatorname{Im}\left(\overline{V}_{s}\overline{I}_{s,g}^{*}\right) + Q_{g,set}$$
(25)

Eqs. (20)-(25) are linearized in (26), and solved iteratively to find the voltages and the windings' currents of the DFIG, where J is the Jacobian matrix.

$$\begin{bmatrix} \Delta P_{\rm M} \\ \Delta Q_{\rm s} \\ \Delta P_{\rm m} \\ \Delta Q_{\rm m} \\ \Delta P_{\rm g} \\ \Delta Q_{\rm g} \end{bmatrix} + J \begin{bmatrix} \Delta \theta_{\rm m} \\ \Delta V_{\rm m} \\ \Delta \theta_{\rm r} \\ \Delta V_{\rm r} \\ \Delta \theta_{\rm g} \\ \Delta V_{\rm g} \end{bmatrix} = \begin{bmatrix} 0 \\ 0 \\ 0 \\ 0 \\ 0 \\ 0 \end{bmatrix}$$

$$(26)$$

With $P_{s,m}$, $Q_{s,m}$, $P_{s,g}$, and $Q_{s,g}$, P_{DFIG} is given in (27), with exact correspondence to v_w . Then (3), (8), and (9) are solved to find the RPL of the DFIG (28).

$$P_{\rm DFIG} = -P_{\rm s,m} - P_{\rm s,g} \tag{27}$$

$$\begin{cases} Q_{DFIG,max} = max(-Q_{s,m}) + max(-Q_{s,g}) \\ Q_{DFIG,min} = min(-Q_{s,m}) + min(-Q_{s,g}) \end{cases}$$
 (28)

The RPL based on detailed solution to the DFIG is more exact than that the existing model, since simplified definition of the slip power is not used. But it still has some errors,

- 1) The RPL is related to P_{DFIG} , and P_{DFIG} is solved from $Q_{\mathrm{DFIG,set}}$, but $Q_{\mathrm{DFIG,set}}$ is not equal to $Q_{\mathrm{DFIG,max}}$ or $Q_{\mathrm{DFIG,min}}$, thus the PRL is not consistent with the initial reactive power setting to Q_{DFIG} . In other words, different $Q_{\mathrm{DFIG,set}}$ will yield different RPL, which is obviously wrong.
- 2) The DFIG's RPL is related to V_s , but V_s is decided by $V_{\rm PCC}$ and the outputs of other DFIGs, thus not fixed.
- 3) A wind farm often has tens of DFIGs in several strings. For system-side analysis, RPL of wind farm is more valuable than those of the DFIGs. Due to power loss of collectors, power output of wind farm $P_{\rm WF}+jQ_{\rm WF}$ is not equal to the sum of $P_{\rm DFIG}+jQ_{\rm DFIG}$. RPL model of wind farm based on solution to DFIGs and collectors has not been found.

3.2. RPL model of DFIG consistent with QDFIG

To solve the problem 1), an iterative solution to the RPL of the DFIG is proposed in Fig. 7, with $Q_{\rm DFIG,set}$ replaced by $Q_{\rm DFIG,max}$ (or $Q_{\rm DFIG,min}$) repeatedly. It has 3 steps,

- a. From a positive $Q_{DFIG,set}$, solve the DFIG with (27).
- b. With (3), (8) and (9), P_{DFIG} , $Q_{DFIG,max}$ and $Q_{g,max}$ are found.
- c. If the difference of $Q_{\mathrm{DFIG,set}}$ and $Q_{\mathrm{DFIG,max}}$ is larger than a criterion ε , set $Q_{\mathrm{DFIG,set}} = Q_{\mathrm{DFIG,max}}$, $Q_{\mathrm{g,set}} = Q_{\mathrm{g,max}}$, and go to step a. Otherwise, $Q_{\mathrm{DFIG,max}}$ is found, and the iteration stops.

Similarly, from a negative $Q_{\mathrm{DFIG,set}}$, $Q_{\mathrm{DFIG,min}}$ will be derived. Although the RPL is solved from $Q_{\mathrm{DFIG,set}}$, it is independent of the latter. With the same v_{w} and V_{s} , different $Q_{\mathrm{DFIG,set}}$ yield the same $Q_{\mathrm{DFIG,max}}$ and $Q_{\mathrm{DFIG,min}}$.

If the DFIG operates at the synchronous speed, the junction temperature rise due to dc rotor current should be considered in deciding the RPL [26,27]. Such DFIG is similar to the SG, but the solution is different. For the SG, the knowns are the stator power and stator power at stator side, and the unknowns are field voltage, current, and mechanical power at rotor side. For such DFIG, the mechanical power and the reactive power at both the stator and the rotor sides are known, and the unknowns are also at both sides. The RPL of such DFIG may also be quantified following Fig. 7.

It should be noted that when solving the RPL of the DFIG, there is no limit to the Cp function or the DFIG configuration. For the DFIG with different type, after replacing the Cp function or the configuration parameters, the proposed model is still applicable.

4. RPL model of wind farm and its PQ dependence

4.1. RPL model of wind farm

To the problems 2) and 3), the wind farm with DFIGs and collectors is

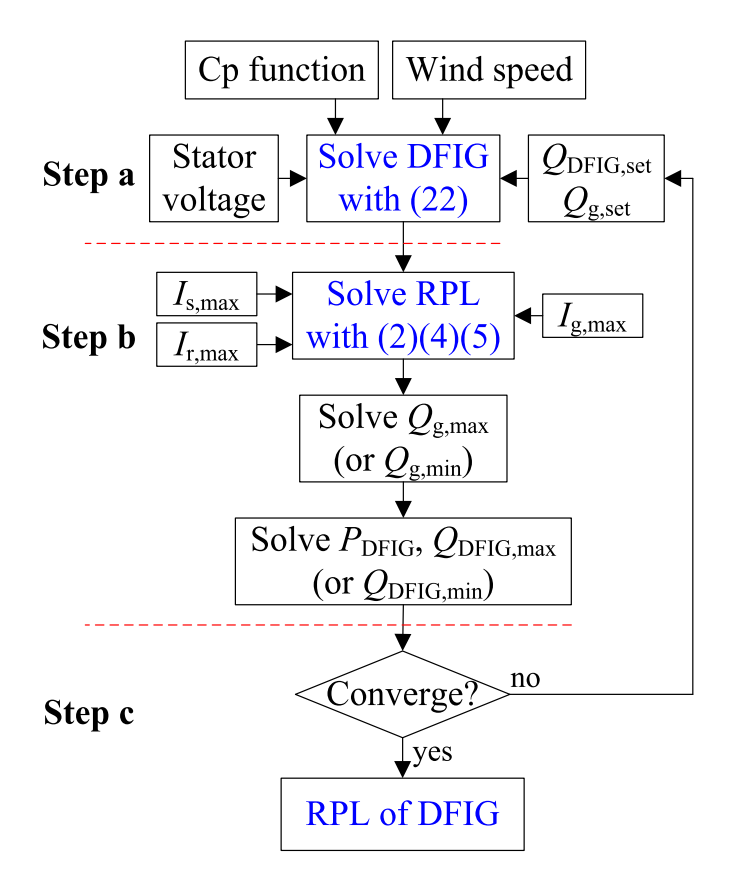


Fig. 7. Solution to RPL of DFIG with consistence to $Q_{\rm DFIG}$.

solved. Since the impedances of DFIGs are often much larger than those of the collectors, simultaneous solution to DFIGs and collectors may diverge. Hence considering the impact of $V_{\rm PCC}$ on $V_{\rm S}$, the RPLs of DFIGs and the power flow of wind farm are solved alternatively to derive the RPL of the wind farm.

With the DFIGs at their RPL, power flow equations of the collectors in (29) are linearized to (30), as solved iteratively to update the stator voltages, where \boldsymbol{G} is the conductance matrix, \boldsymbol{B} is the susceptance matrix, \boldsymbol{i} , \boldsymbol{j} denote the bus, the subscript L and C denote the load and the collector respectively. For the bus without DFIG, $P_{\text{DFIG}}=0$ and $Q_{\text{DFIG}}=0$. For the bus without load, $P_{\text{L}}=0$ and $Q_{\text{L}}=0$.

$$\begin{cases} \Delta P_i = P_{\text{DFIG},i} - P_{\text{L},i} - V_i \sum_j V_j (G_{i,j} \cos \theta_{i,j} + B_{i,j} \sin \theta_{i,j}) = 0 \\ \Delta Q_i = Q_{\text{DFIG},i} - Q_{\text{L},i} - V_i \sum_j V_j (G_{i,j} \sin \theta_{i,j} - B_{i,j} \cos \theta_{i,j}) = 0 \end{cases}$$
(29)

$$\begin{bmatrix} \Delta P_{\rm C} \\ \Delta Q_{\rm C} \end{bmatrix} + \begin{bmatrix} J_{P,\theta} & J_{P,V} \\ J_{Q,\theta} & J_{Q,V} \end{bmatrix} \begin{bmatrix} \Delta \theta_{\rm C} \\ \Delta V_{\rm C} \end{bmatrix} = \begin{bmatrix} \mathbf{0} \\ \mathbf{0} \end{bmatrix}$$
(30)

With V_s , the RPLs of the DFIGs are solved. Then the power flow of the collectors is solved again. The process is repeated until $P_{\rm WF}$ and $Q_{\rm WF}$ of wind farm converge, as shown in Fig. 8. The resultant $Q_{\rm WF}$ is the RPL of the wind farm.

$$\begin{cases} Q_{\text{WF,max}} = Q_{\text{WF}}|_{Q_{\text{DFIG}} = Q_{\text{DFIG,max}}} \\ Q_{\text{WF,min}} = Q_{\text{WF}}|_{Q_{\text{DFIG}} = Q_{\text{DFIG,min}}} \end{cases}$$
(31)

The alternative solution has two merits, 1) Since the DFIGs are solved separately, different $v_{\rm w}$ are allowed for the DFIGs. 2) Solution with the Newton method allows the collectors to be radial or with a few loops. The latter is to improve reliability of wind farm against outage of collector [28,29].

One may doubt if RPLs of the DFIGs and power flow of the collectors may be solved simultaneously to save calculation effort. But it is difficult to solve an optimum problem and a set of nonlinear equations together,

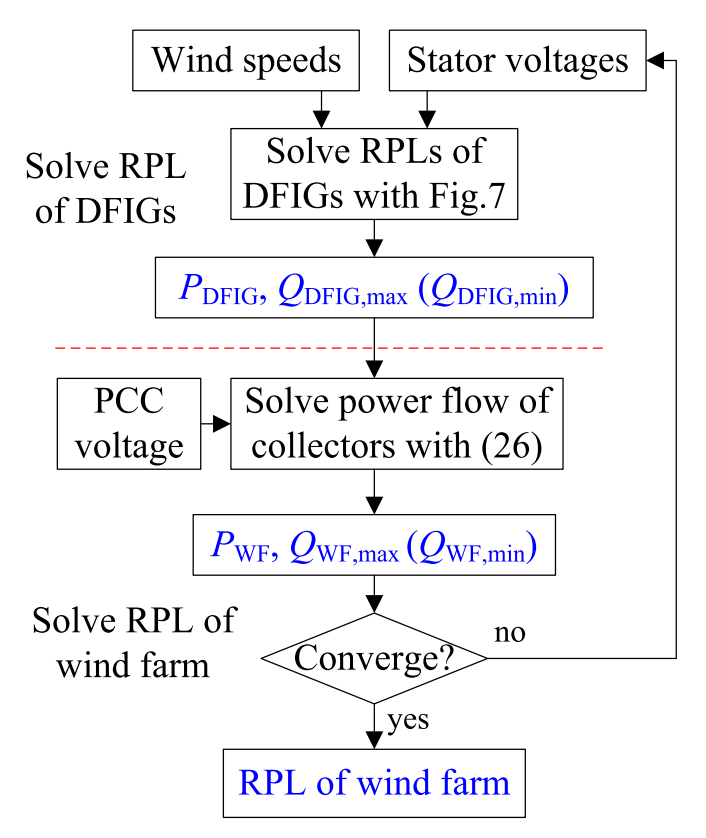


Fig. 8. Alternative solution to RPL of wind farm.

and the solution may diverge as explained earlier.

When solving the RPL of the wind farm, by using the Newton power flow, the proposed model has no limit on the configuration of the collector network, i.e. the latter may be radial or looped. The only assumption is that the PCC voltage is known.

4.2. Dependence of active power of wind farm on the RPL

The RPL of wind farm has some new characteristics.

- (1) The voltage levels of the DFIG and collector are lower than those of the SG and transmission line, hence the active power loss of the wind farm is relatively large and can not be ignored. Considering the power loss, the RPL of wind farm is different from the sum of the RPLs of the DFIGs.
- (2) Due to the reactive power loss of the magnetizing circuit of the DFIG, the RPL of wind farm is not symmetrical about the horizontal axis (32), as seen in Fig. 9(a).

$$|Q_{\text{WF,max}}| < |Q_{\text{WF,min}}| \tag{32}$$

The more reactive power produced (or absorbed), the larger active power loss. So from (32), one gets (33). Consequently, even though $v_{\rm W}$ and $V_{\rm PCC}$ do not change, $Q_{\rm WF,max}$ and $Q_{\rm WF,min}$ at the RPL yield two $P_{\rm WF}$, as shown with points A and B in Fig. 9 (b).

$$P_{\text{WF}}|_{Q_{\text{WF,max}}} > P_{\text{WF}}|_{Q_{\text{WF,min}}} \tag{33}$$

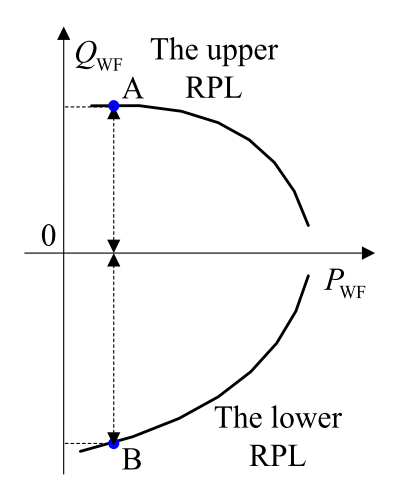
One may doubt if the DFIG or SG also has 2 active powers at its RPL. The answer is yes. As illustrated in Fig. 10, with the same active power P_1 , P_2 is given by (34), which is a quadric function of Q_2 , thus P_2 varies with Q_2 . Hence in Figs. 7 and 8, $P_{\rm DFIG}$ is solved from $Q_{\rm DFIG,max}$ and $Q_{\rm DFIG}$, min separately to find the RPL of wind farm. For the SG, $R_{\rm S}$ is small, thus difference of $P_{\rm SG}$ due to $Q_{\rm SG}$ is often ignored.

$$P_2 = P_1 - \frac{P_2^2 + Q_2^2}{IT^2} R \tag{34}$$

To show change of P_{WF} due to different Q_{WF} , two indices ξ_1 and ξ_2 are newly defined in (35) and (36), where ξ_1 shows the difference of the max/min P_{WF} between the upper/lower RPL, and ξ_2 quantifies the difference of P_{WF} at the upper/lower RPL.

$$\xi_1 = \frac{\left| P_{\text{WF,C}} - \min(P_{\text{WF,A}}, P_{\text{WF,B}}) \right|}{P_{\text{WF,C}}} \tag{35}$$

$$\xi_{2} = \frac{\max(P_{\text{WF,A}}, P_{\text{WF,B}}) - \min(P_{\text{WF,A}}, P_{\text{WF,B}})}{\max(P_{\text{WF,A}}, P_{\text{WF,B}})}$$
(36)



(a) Imbalanced RPL curve

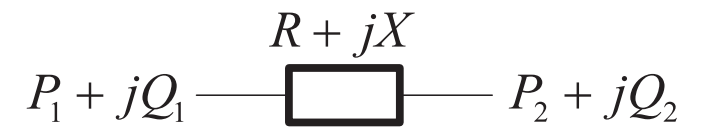


Fig. 10. Explanation to two solutions to P_{DFIG} or P_{SG} .

4.3. Data fitting to dependence of PWF on the RPL

To describe the dependence of P_{WF} on Q_{WF} , more point, e.g. point C with $Q_{DFIG} = 0$, is added in Fig. 9(b). Often there exists,

$$\begin{cases}
|Q_{\text{WF,C}}| < Q_{\text{WF,A}} < |Q_{\text{WF,B}}| \\
P_{\text{WF,B}} < P_{\text{WF,A}} < P_{\text{WF,C}}
\end{cases}$$
(37)

With points A, B, and C, relation of $P_{\rm WF}$ and $Q_{\rm WF}$ is fit to a quadric function (38), as shown with red dotted curve in Fig. 9 (b), where the coefficients a_0 , a_1 , and a_2 are decided by (39).

$$P_{WF} = a_0 + a_1 Q_{WF} + a_2 Q_{WF}^2 \tag{38}$$

$$\begin{bmatrix} a_0 \\ a_1 \\ a_2 \end{bmatrix} = \begin{bmatrix} 1 & Q_{WF,A} & Q_{WF,A}^2 \\ 1 & Q_{WF,B} & Q_{WF,B}^2 \\ 1 & Q_{WF,C} & Q_{WF,C}^2 \end{bmatrix}^{-1} \begin{bmatrix} P_{WF,A} \\ P_{WF,B} \\ P_{WF,C} \end{bmatrix}$$
(39)

Finally for given $v_{\rm w}$ and PCC voltage, dependence of $P_{\rm WF}$ on the RPL of wind farm is given by,

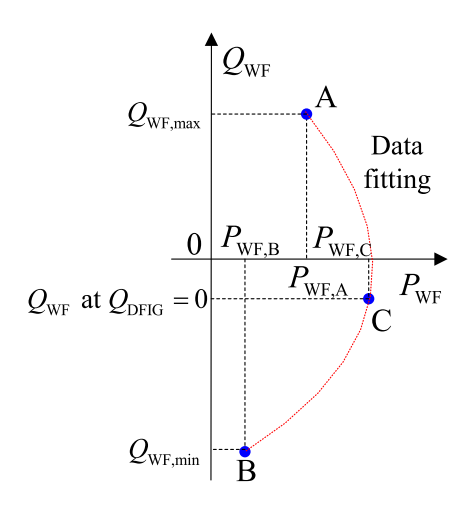
$$\begin{cases}
P_{WF} = a_0 + a_1 Q_{WF} + a_2 Q_{WF}^2 \\
Q_{WF,min} < Q_{WF} < Q_{WF,max}
\end{cases}$$
(40)

Finally, the process to solve the RPL of wind farm and quantify the dependence is shown in Fig. 11.

4.4. Discussions

The RPL of wind farm is based on V_{PCC} . For power flow or power dispatch, V_{PCC} changes with the wind speed and system condition. To show the impact of V_{PCC} on the RPL of the wind farm, there are two choices:

(a) Find the sensitivities of P_{WF} , $Q_{\mathrm{WF,max}}$, and $Q_{\mathrm{WF,min}}$ with respect to V_{PCC} . Analytical sensitivity model is difficult, since P_{WF} and Q_{WF} are solved with the alternative solution instead of simultaneous solution. The analytical Q-V sensitivity with the alternative solution to the DFIGs



(b) Two P_{WF} at the RPL

Fig. 9. P_{WT} at the RPL of wind farm.

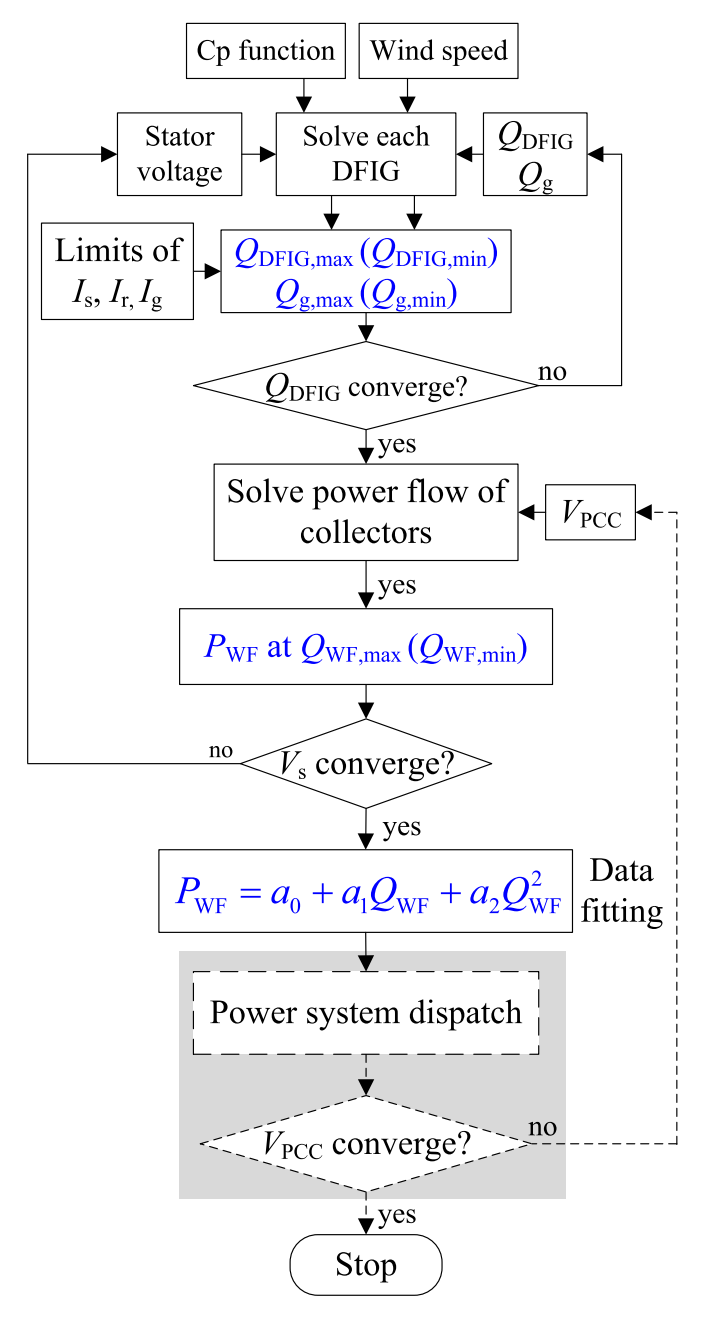


Fig. 11. Quantifying dependence of P_{WF} one the RPL of wind farm.

and collectors is proposed in [6]. But the sensitivity here is more complex, since there are more alternative solutions. Thus the perturbation method may be used to find the sensitivity of the RPL of wind farm with respect to the PCC voltage.

For nonlinear curve y = f(x), the operation point is given by (x_0, y_0) . If x increases by Δx , the corresponding change of y is Δy . If Δx is small enough, i.e. the tangent, of the curve at (x_0, y_0) is given by,

$$\xi = \lim_{\Delta x \to 0} \frac{\Delta y}{\Delta x} \tag{41}$$

The perturbation method is easy to use. It is accurate if Δx is small enough. For practical application, it has two drawbacks, (1) For actual calculation, Δx can not approach 0, and there is truncation error. (2) The perturbation method is suitable for one curve and one parameter, but troublesome for multiple curves with more than one parameter, i.e. $\mathbf{y} = \mathbf{f}(x)$, where $\mathbf{y} = [y_1, y_2, ..., y_n]^T$, $\mathbf{x} = [x_1, x_2, ..., x_n]^T$, and the subscript T denotes the transpose.

(b) Add an outer iteration of system-side analysis with the interface of $V_{\rm PCC}$, as shown with the shadowy blocks in Fig. 11. Compared with the perturbation method, it is more accurate, but computationally more expensive.

The DFIG has several windings, their stator voltages are not fixed, and the collectors may have radial or loop structure, so it seems that the quadric curve is rough, and more points may be used for more exact PQ relation, but it is difficult. At points A or B, $P_{\rm WF}$ strictly corresponds to $Q_{\rm DFIG,max}$ or $Q_{\rm DFIG,min}$. With $Q_{\rm DFIG,set}$ and $Q_{\rm g,set}$ of 0, point C yields a unique $P_{\rm WF}$ and $Q_{\rm WF}$, thus there is only a RPL curve for given $v_{\rm W}$ and $V_{\rm PCC}$. But each $Q_{\rm WF}$ corresponds to different schemes of $Q_{\rm DFIG,set}$ $Q_{\rm g,set}$, thus numerous RPL curves.

The proposed RPL model is based on alternative solution, suitable to other distributed generators, e.g. permanent-magnet SG, photovoltaic unit, energy storage [30,31], with the only difference of solution process to the equipment.

The RPL models of the SGs and the DFIGs are usually power flow or optimal power flow (economic dispatch) analysis. Compared with those the DFIG and the wind farm, the existing RPL model of the SG is easier and more simplified, since the mechanical power of the SG is decided by the prime mover and irrelevant to the rotor speed, and the excitation loop with the rectifier powered by the power system [32] is often ignored. When deriving the RPC of the DFIG and the wind farm in this paper, the relation of the captured power of the wind turbine and the power loss of the DFIG with the variable rotor speed and the wind speed is considered. The contribution of the slip power through the B2B converters to the RPL of the DFIG is also included. The only simplification may be that the power loss of the converters is ignored in solving the DFIG and the wind farm. But if necessary, the loss may be given by the product of the resistances multiplied by the square of the stator/rotor currents respectively, which may be easily incorporated in the proposed model.

5. Numerical analysis

The proposed RPL models of the DFIG and wind farm are realized by the Matlab software and run on the computer with Intel Core i7-8700. The DFIG's parameters are given in Table 2 [6,14,15,27]. The current limits of the stator, the rotor, and the GSC are 1.1p.u., 1.1p.u., and 0.6p. u. respectively. Although the rotor speed is decided by the current limit of the converters, the latter in per unit is wider than the former, since the RSC and the GSC produce both active and reactive powers.

In this Section, the DFIG's RPL considering the windings' resistance and consistent with reactive power is derived at first. Then the RPL of wind farm considering the impact of the PCC voltage on the RPLs of the DFIGs is given. Finally, a quadric curve is fit to describe the relation of PQ dependence of the wind farm at its RPL.

5.1. RPL of the DFIG

With $V_s=1$ p.u., the DFIG is solved with $Q_{\mathrm{DFIG,set}}$ repeatedly replaced by $Q_{\mathrm{DFIG,max}}$ (or $Q_{\mathrm{DFIG,min}}$). For different v_{w} , after 4—5 iterations, the limits of the stator, the rotor, and the GSC are shown in Fig. 12, where the base power is the capacity of the DFIG. The limit of the rotor (red curve) is asymmetrical about the horizontal axis. The reason is that the

Table 2 Parameters of the DFIG.

Rated voltage (V)	690	c_3	0.58	$R_{\rm s}$ (p.u.)	0.0078
Rated capacity (MW)	2	c ₄	0.002	<i>X</i> _s (p.u.)	0.0794
Diameter of WT (m)	71	c_5	2.14	$R_{\rm r}$ (p.u.)	0.025
Gear ratio	94	c_6	13.2	$X_{\rm r}$ (p.u.)	0.4
Poles	2	C7	18.4	$X_{\rm m}$ (p.u.)	4.1039
c_1	0.73	c_8	-0.02	$R_{\rm g}$ (p.u.)	0.03
c_2	151	c_9	-0.003	$X_{\rm g}$ (p.u.)	0.05

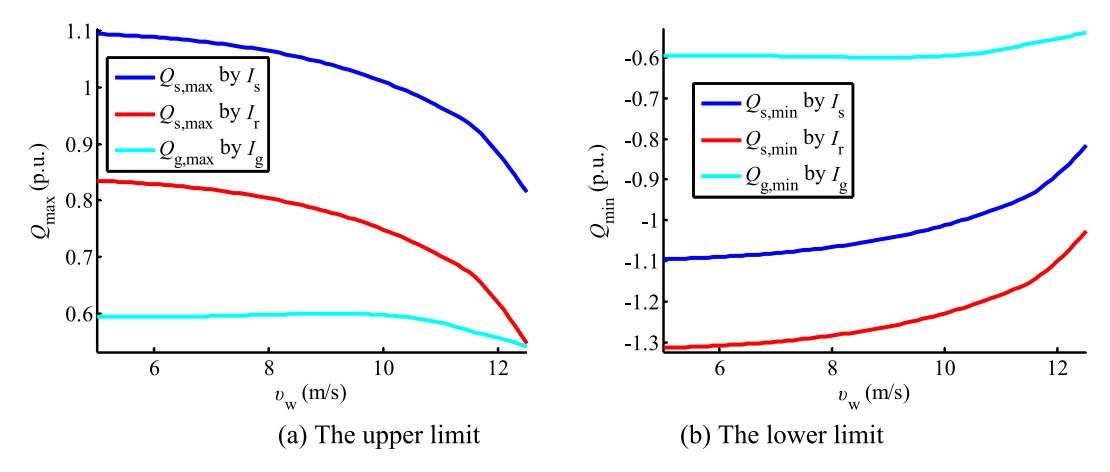


Fig. 12. Limits of the windings of the DFIG.

RPL of the operation region of the stator power constrained by the rotor current limit is not symmetrical, which is consistent with Fig. 3(a). At the upper/lower RPL, $P_{\rm DFIG}$ is shown in Fig. 13(a), and the difference between them is shown in Fig. 13 (b) which is more obvious for lower $v_{\rm w}$.

Based on Fig. 12, the DFIG's RPL is shown in Fig. 14. Compared with Fig. 3 (b), the RPL has exact correspondence to $v_{\rm w}$, s, and $P_{\rm DFIG}$. With the higher $V_{\rm s}$, the same power needs less current, thus the RPL is wider. Hence due to power flow direction, the DFIG at the end of the string and far away from the PCC has higher stator voltage, and its RPL is wider. Since $V_{\rm s}$ changes with $V_{\rm PCC}$ and outputs of other DFIGs, the DFIG RPL with a fixed $V_{\rm s}$ is of little value for the wind farm and the power system.

For $v_{\rm W}=10$ m/s, solution process to the DFIG's RPL is given in Table 3. It is found that the RPL is independent of $Q_{\rm DFIG,set}$. $P_{\rm DFIG}$ at $Q_{\rm DFIG,max}$ is less than that at $Q_{\rm DFIG,min}$, with the error of 0.0063p.u., or 1.29 %. Since the iterations converge quickly, 2—3 iterations are enough to find the RPL For practical use.

To verify the error of the existing RPL model, μ defined in (16) is given in Table 4. It is about -0.03p.u. at the upper RPL, and -0.02p.u. at the lower RPL. It is found that $|\mu/P_{\rm em}|$ is more notable for lower $v_{\rm w}$. At the upper RPL with $v_{\rm w}=5$ m/s, $|\mu/P_{\rm em}|$ is 27.48 %. Thus the slip power ignoring the windings' resistance is inaccurate for deriving the RPL of the DFIG.

5.2. RPL of wind farm and its PQ dependence

The wind farm in Fig. 15 has 4 strings, 38 DFIGs. The total capacity is 76 MW [6]. Since the RPL is independent of the reactive power settings,

 $Q_{\mathrm{DFIG,set}}=0.02$ p.u. and $Q_{\mathrm{g,set}}=0.01$ p.u. The impedance of the collectors is $0.05+\mathrm{j}0.12\,\Omega/\mathrm{km}$. The PCC voltage is 1.05p.u. The number of DFIGs, the impedance of the collectors, and the rated voltage at the PCC are chosen with the following considerations,

- 1) The number of the DFIGs in one string is decided by not only the capacities of the cables and the step-up transformer, but also rise of the stator voltage of the DFIGs at the end of the strings. For example, # 21 DFIG is more vulnerable to overvoltage than # 10 DFIG. The number of strings in a wind farm is decided by the capacity of the step-up transformer at the PCC.
- 2) The higher rated PCC voltage may allow more and larger DFIGs in the wind farm, but there is no standard rule. Usually small wind farm has tens of WTGs, thus the PCC voltage is low, e.g. 10 kV. Large wind farms (i.e. wind power base) may have the capacity of GW, and may be stepped up to 110 kV, 220 kV, or higher-voltage grid.
- 3) The unit-length impedance of the collectors is decided by its rated voltage (35 kV). The lengths of the cables are decided by the location for the DFIG determined by wind resource, and also the power loss and voltage drop along the cables.

To solve the RPL of wind farm in complex scenario, $v_{\rm W}$ are set different. Under the MPPT mode, wind farm with the DFIGs at their upper RPL is solved. Fig. 16(a) gives $P_{\rm WT}$ of the DFIGs, with total value of $\sum P_{\rm WT} = 40.2108$ MW. It is found that the higher $v_{\rm W}$, the larger $P_{\rm WT}$, unless the DFIGs reach their power limit. Fig. 16 (b) shows the slips and the RSC voltage angles. Most DFIGs have high $v_{\rm W}$ and oversynchronous speed, thus s is negative. For the #25, #27–29 DFIGs, $v_{\rm W}$ are low, thus s

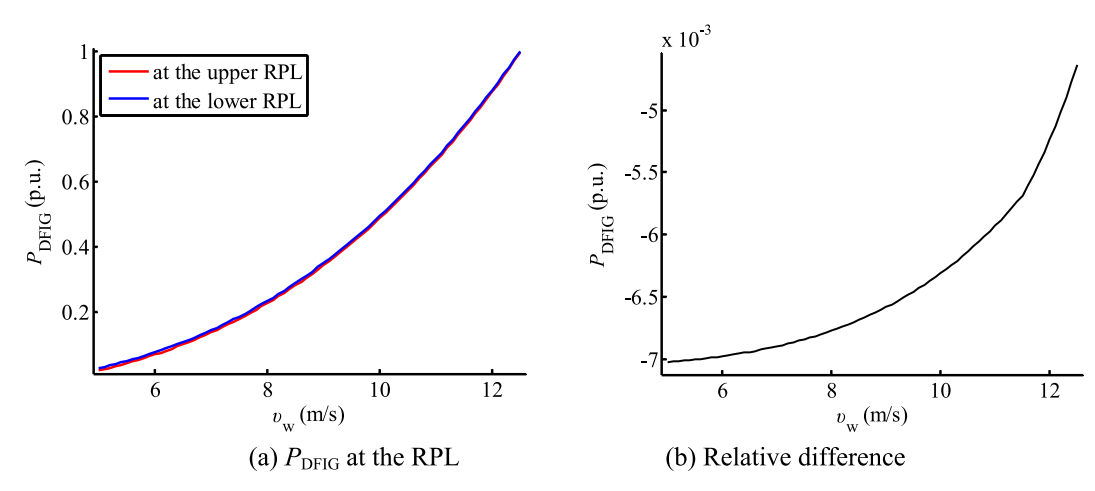


Fig. 13. P_{DFIG} at the upper and lower RPL.

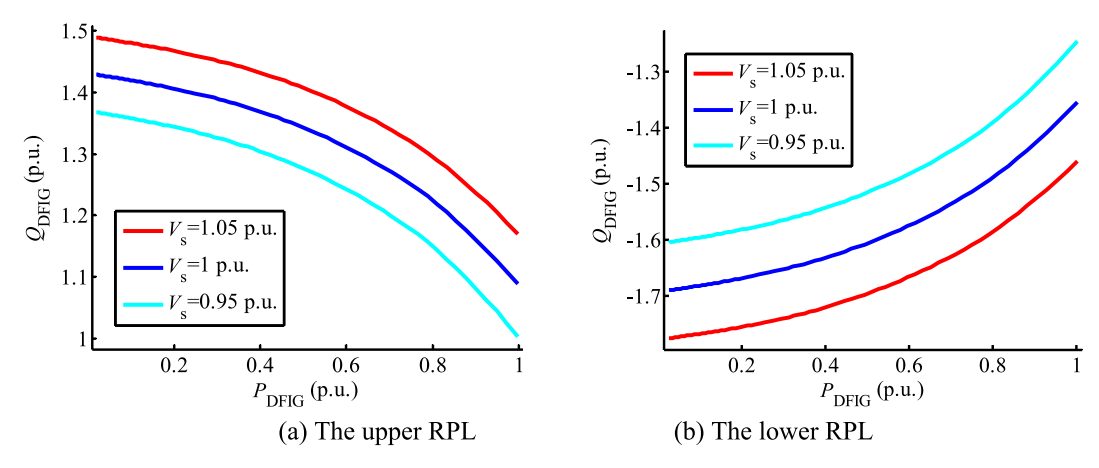


Fig. 14. The RPL of the DFIG with different wind speeds and stator voltages.

Table 3 Iterative solution to RPL of DFIG with consistence to $Q_{\rm DFIG}$.

Q _{DFIG,set} Iteration		The upper RPL		The lower RPL	
(p.u.)		Q _{DFIG,max} (p.u.)	P _{DFIG} (p.u.)	Q _{DFIG,min} (p.u.)	P _{DFIG} (p.u.)
0.2 or	1	0.2	0.524853	-0.2	0.527324
-0.2	2	1.340598	0.488303	-1.602095	0.494660
	3	1.346261	0.488051	-1.608630	0.494362
	4	1.346292	0.488050	-1.608678	0.494360
0.3 or	1	0.3	0.522615	-0.3	0.527557
-0.3	2	1.340988	0.488287	-1.602126	0.494657
	3	1.346263	0.488051	-1.608630	0.494362
	4	1.346292	0.488050	-1.608678	0.494360

Table 4 Error of existing RPL model using the simplified slip power.

	υ _w (m/ s)	S	–P _{r,m} (p.u.)	P _{em} (p.u.)	μ (p.u.)
At the upper	6	0.271187	-0.073249	-0.158546	-0.030254
RPL	8	0.028040	-0.038158	-0.281799	-0.030256
	10	-0.214480	0.064214	-0.440481	-0.030260
	12	-0.400000	0.233850	-0.660288	-0.030265
At the lower	6	0.271187	-0.062380	-0.158546	-0.019385
RPL	8	0.028040	-0.027588	-0.281799	-0.019687
	10	-0.214480	0.074117	-0.440481	-0.020358
	12	-0.400000	0.242197	-0.660288	-0.021918

is positive. Based on the author's experience, the sign of s helps to decide the initial value of $\theta_{\rm r}$ to avoid divergence.

The stator voltages and the power outputs of the DFIGs are shown in Fig. 16(c) and (d). It is found that $V_{\rm S}$ is larger than $V_{\rm PCC}$ with the DFIGs at the upper RPL limit. The reason is that active and reactive powers of DFIGs increase the voltage drop to the PCC, which is more obvious for the string 2 with more DFIGs. Hence the existing RPL model of the DFIG with fixed $V_{\rm S}$ is too ideal to be of any value. It is also found that $Q_{\rm DFIG}$, max varies with $P_{\rm DFIG}$, especially when $v_{\rm W}$ is large and $P_{\rm DFIG}$ is near the rated value, which validates the necessity of exact solution to $P_{\rm DFIG}$ as ignored by existing RPL model.

Similarly, the lower RPL of the wind farm with the DFIGs at the lower RPL is solved as shown in Fig. 17. Compared with Fig. 16, one distinct difference is that stator voltages are much lower. At the lower RPL, the reactive power is negative, i.e. flowing from PCC to the DFIG and counteracting the voltage drop caused by active power from the stator to the PCC, thus $V_{\rm S}$ is lower than $V_{\rm PCC}$. The asymmetrical of the RPL of the wind farm is due to not only the asymmetry of the RPLs of the DFIGs, but also the reactive power loss in the transformers and the collectors. Above asymmetry will yield not only error of the RPL of the DFIG or the wind farm, but also mismatch of the P-O relation.

With the DFIGs at the upper or the lower RPL, the RPL of the wind farm is given in Table 5, which shows that at the upper RPL, conversion efficiency to active power of the DFIGs is about 91 %, and transmission efficiency of the collectors is about 86 %. At the lower RPL, the data are 92 % and 80 % respectively. With reactive power absorbed instead of produced by the DFIGs, conversion efficiency of the DFIGs increases, but that of the collectors decreases.

With $v_{\rm w}$ of the DFIGs do not change (but they are different, as shown

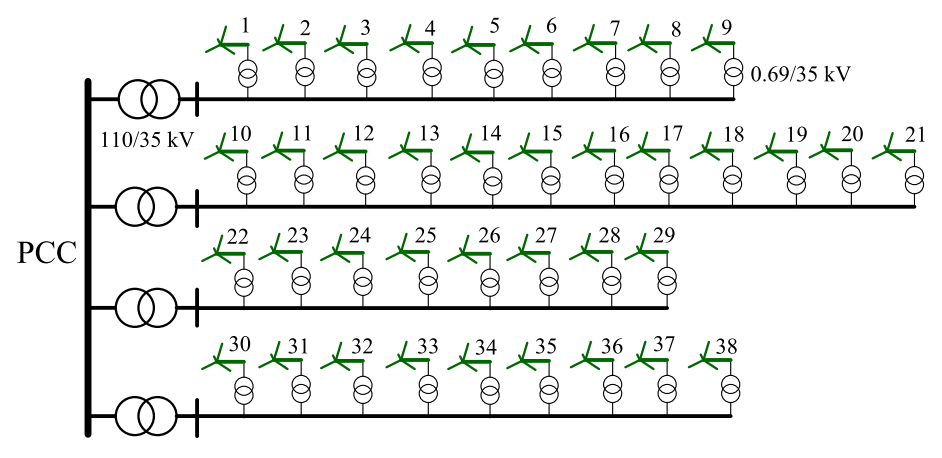


Fig. 15. Wind farm with DFIGs and collectors.

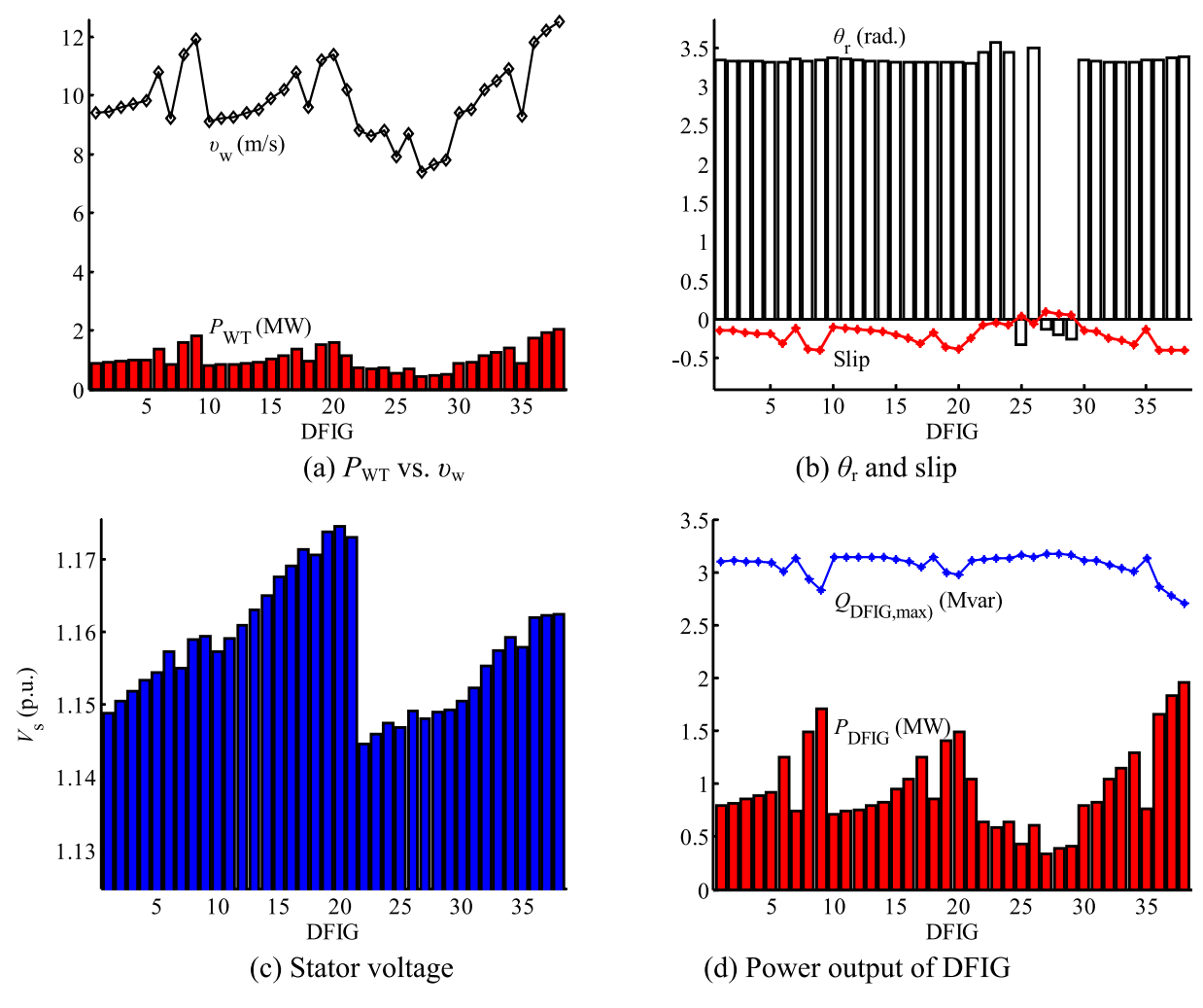


Fig. 16. Wind farm solution with DFIGs at their upper RPL.

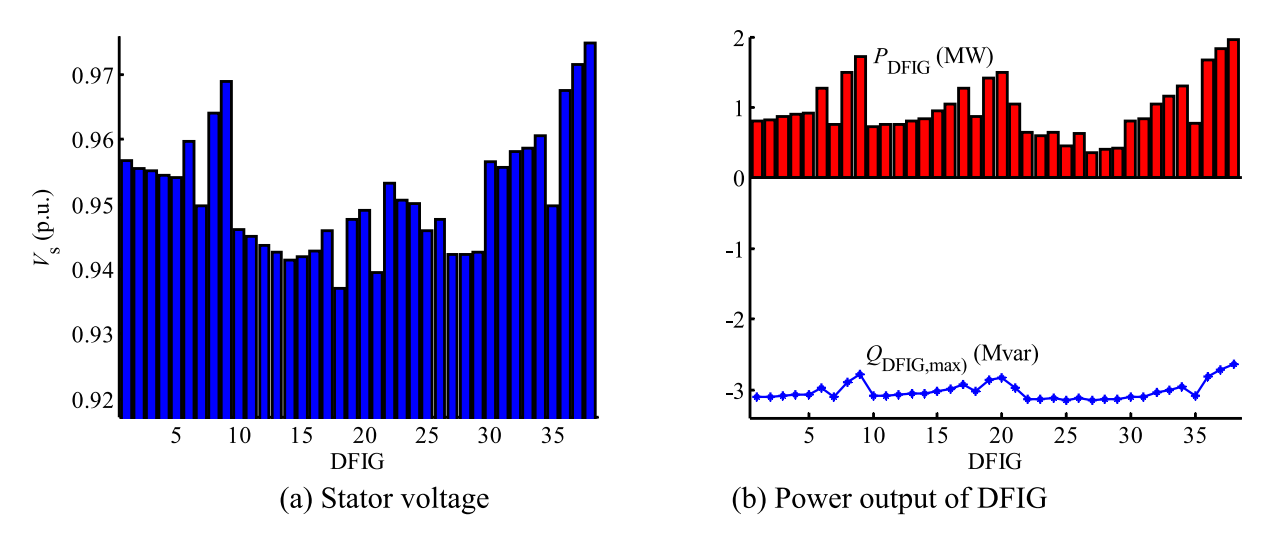


Fig. 17. Wind farm solution with DFIGs at their lower RPL.

in Fig. 16(a)), the absolute value of the lower RPL (e.g. 129.8935 Mvar at $V_{\rm PCC}=1.05 {\rm p.u.}$) of wind farm is obviously larger than that of the upper RPL (106.0935 Mvar), yielding 2 $P_{\rm WF}$ (29.6835 MW and 31.5604 MW respectively).

The sensitivity analysis may show more insight to the RPL modelling, thus discussed here, $\,$

(1). Different configuration of the collector network changes the admittance matrix, but adds no difficulty to solve the Newton power flow in (29) and (30). It should be noted that the maximum strings in the wind farm is decided by the step-up transformer at the PCC, and the maximum number of the DFIGs in one string is decided by the capacity of the step-up transformer at the DFIG,

Table 5Power output of wind farm at its RPL.

V _{PCC} (p.u.)	Scheme	$\sum P_{\mathrm{DFIG}}$ (MW)	$\sum Q_{\mathrm{DFIG}}$ (Mvar)	P _{WF} (MW)	Q _{WF} (Mvar)
1.05	Upper RPL	36.6853	116.5807	31.5604	106.0935
	Lower RPL	37.0766	-114.7638	29.6835	-129.8925
1.02	Upper RPL	36.6779	113.8550	31.5060	103.2717
	Lower RPL	37.0492	-110.7130	29.6696	-125.8140
1.00	Upper RPL	36.6730	112.0135	31.4699	101.3664
	Lower RPL	37.0307	-108.0054	29.6609	-123.0862

the capacity of the cable, and also overvoltage risk of the DFIG at the far end of the string, thus the string can not be very long. The location of the DFIGs and the topology of the collectors are decided by the wind resource. In other words, the configuration of the wind farm can not be deliberately set.

- (2). Change of the wind speeds only affects (17)-(19), which is quite easy. Due to the terrain and wake effects, it is often not suitable to set the same wind speeds for all the DFIGs. As seen in Fig. 16(a), wind speeds of the DFIGs in the wind farm are different, which yields different parameters of the DFIGs. The sensitivity may be observed by comparing the parameters of the DFIGs with different wind speeds in Figs. 16 and 17.
- (3). The slip is not an independent variable, but decided by the wind speed under the MPPT mode, and also decided by the power setting under the derated mode. Hence sensitivity analysis to it is not practical.
- (4). The power loss of the converters is ignored in solving the DFIG and the wind farm. But if necessary, the loss may be given by the product of the resistances multiplied by the square of the stator/ rotor currents respectively, which may be easily incorporated in the proposed model.
- (5). To quantify the dependence of the RPL on V_{PCC} , the latter is set to 1.02p.u. and 1p.u. respectively. With smaller V_{PCC} , it is found from Table 5 that,
- (a) $\sum Q_{\mathrm{DFIG}}$ and Q_{WF} decrease at the upper RPL and increase at the lower RPL, hence the operational ranges of the DFIGs and wind farm are narrower with lower V_{PCC} . The sensitivity of $Q_{\mathrm{WF,max}}$ with respect to V_{PCC} is about 95 Mvar/p.u., and the sensitivity of $Q_{\mathrm{WF,min}}$ with respect to V_{PCC} is -136 Mvar/p.u., i.e. the lower RPL of the wind farm is more sensitive to V_{PCC} .
- (b) ∑P_{DFIG} and P_{WF} decrease at both the upper and the low RPL. The sensitivity of P_{WF} with respect to V_{PCC} is about 1.8 MW/p.u. at the upper RPL, and 0.4 MW/p.u. at the lower RPL. Hence P_{WF} at the upper RPL is more sensitive to V_{PCC}.

5.3. Data fitting to active and reactive powers of wind farm

With $Q_{\mathrm{DFIG,set}}$ and $Q_{\mathrm{g,set}}$ of all the DFIGs set to 0, point C in Fig. 9(b) is found, which together with points A and B at the RPL yields the indices ξ_1 and ξ_2 to evaluate the change of P_{WF} due to different Q_{WF} . As seen in Table 6, within the feasible range of Q_{WF} , ξ_1 is larger than 23.5 %, and at

Table 6 Evaluation to dependence of P_{WF} on the RPL.

V _{PCC} (p.u.)	Point	P _{WF} (MW)	Q _{WF} (Mvar)	<i>ξ</i> ₁ (%)	ξ ₂ (%)
1.05	A	31.5604	106.0935	23.69	5.95
	В	29.6835	-129.8925		
	C	38.8983	-1.4450		
1.02	Α	31.5060	103.2717	23.61	5.83
	В	29.6696	-125.8140		
	C	38.8383	-1.5264		
1.00	Α	31.4699	101.3664	23.54	5.75
	В	29.6609	-123.0862		
	C	38.7951	-1.5845		

the upper/lower RPL, ξ_2 is larger than 5.7 %. Considering that $v_{\rm w}$ do not change, difference of $P_{\rm WF}$ is obvious. It is also found that the higher $V_{\rm PCC}$, the larger ξ , thus the larger change of $P_{\rm WF}$ due to $Q_{\rm WF}$.

With the points A, B, and C, the coefficients a_0 , a_1 and a_2 are calculated using (39) as given in Table 7, from which the relation of $P_{\rm WF}$ with $Q_{\rm WF}$ within the RPL of $Q_{\rm WF}$ is shown in Fig. 18. With the lower $V_{\rm PCC}$, the range of the RPL is narrower, and the curve is more nonlinear, i.e. $P_{\rm WF}$ is more dependent on $Q_{\rm WF}$. It should be noted that Fig. 18 seems to be similar to Fig. 4, but is completely different. In Fig. 4, the input of the DFIG, i.e. $P_{\rm WT}$, changes with different $v_{\rm w}$. But in Fig. 18, $v_{\rm w}$ and $P_{\rm WT}$ of the DFIGs do not change, and the change of $P_{\rm WF}$ is caused by different $Q_{\rm DFIG}$ (or the resultant $Q_{\rm WF}$) only.

To show the dependence of $P_{\rm WF}$ on $Q_{\rm WF}$ with different $v_{\rm w}$, set $V_{\rm PCC}=1.05{\rm p.u.}$, and $v_{\rm w}$ of all the DFIGs are the same, e.g. $v_{\rm w}=5,\ldots$, or $12~{\rm m/s}$ respectively. The relation of $P_{\rm WF}$ on $Q_{\rm WF}$ within the RPL of the wind farm is shown in Fig. 19, and ξ are given in Table 8. With lower $v_{\rm w}$, $P_{\rm WF}$ is smaller and more dependent on $Q_{\rm WF}$, and ξ is larger, i.e. using the same $P_{\rm WF}$ at the upper and the lower RPL of wind farm for the system-side analysis will yield more notable error.

6. Conclusions

In this paper, the reactive power limit model of the DFIG is improved and that of wind farm is proposed. The former avoids the error of the existing models, e.g. (a) ignoring the relation of wind speed, slip, and active power, (b) using simplified slip power ignoring windings' resistance, (c) the reactive power limit inconsistent with initial reactive power of the DFIG. The latter solves the reactive power limit of the DFIGs and power flow of the collectors alternatively, with the PCC voltage instead of the stator voltage fixed. It is newly found that even though wind speeds and the PCC voltage do not change, the upper/lower reactive power limit of wind farm yield two active powers, i.e. $P_{\rm WF}$ is dependent on the reactive power limit, as evaluated with two new indices, and described by a quadric function. Some conclusions are given as follows.

- (1). With $P_{\rm WT}$ seen as $P_{\rm DFIG}$, the active power of the DFIG is overestimated, and the reactive power limit is underestimated. The reactive power limit based on the simplified slip power ignoring the windings' loss yields the error as quantified by the index μ of -0.03p.u. at the upper limit and -0.02p.u. at the lower limit.
- (2). With different wind speeds and considering power flow of the collectors, the stator voltages of the DFIGs are far from the same, thus the reactive power limit of wind farm can not be derived from those of the DFIGs with fixed stator voltages.
- (3). With wind farm at the lower instead of the upper reactive power limit, conversion efficiency of the DFIGs increases, while that of the collectors decreases. The range of the lower limit of wind farm is obviosuly larger than that of the upper limit, which yields 2 acive power of wind farm without changing the wind speed or PCC voltage. Within the reactive power limit, the difference of $P_{\rm WF}$ is larger than 20 %. At the upper/lower reactive power limit, the difference of $P_{\rm WF}$ is larger than 5 %. Hence using the same $P_{\rm WF}$ at the upper and the lower reactive power limit of the wind farm will yield notable error.
- (4). With lower V_{PCC} , the operational region of wind farm is narrower, and the lower limit is more sensitive to V_{PCC} . P_{WF} decreases at the upper and the low limit, P_{WF} at the upper limit is more sensitive to

Table 7Coefficients to describe the PQ dependence.

$V_{\rm PCC}$ (p.u.)	a_0	a_1	a_2
1.05 1.05 1.00	38.9129 38.8555 38.8142	9.24×10^{-3} 1.02×10^{-2} 1.19×10^{-2}	$-6.20 imes 10^{-4} \ -6.57 imes 10^{-4} \ -6.83 imes 10^{-4}$

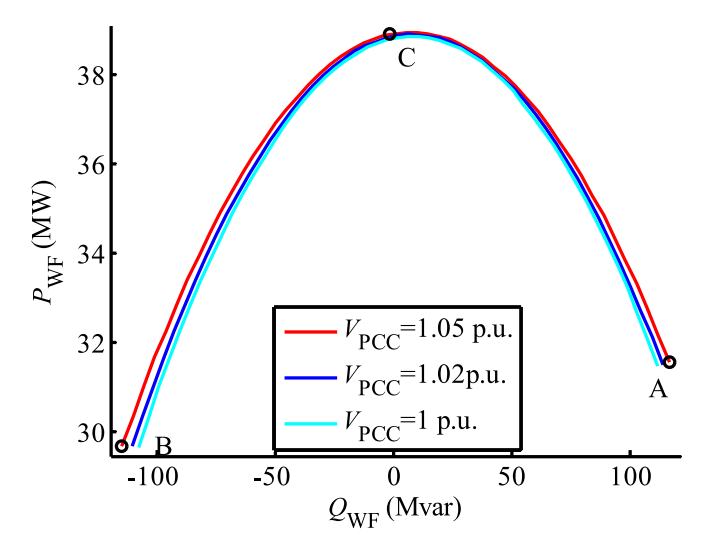


Fig. 18. Relation of P_{WF} with Q_{WF} with different V_{PCC} .

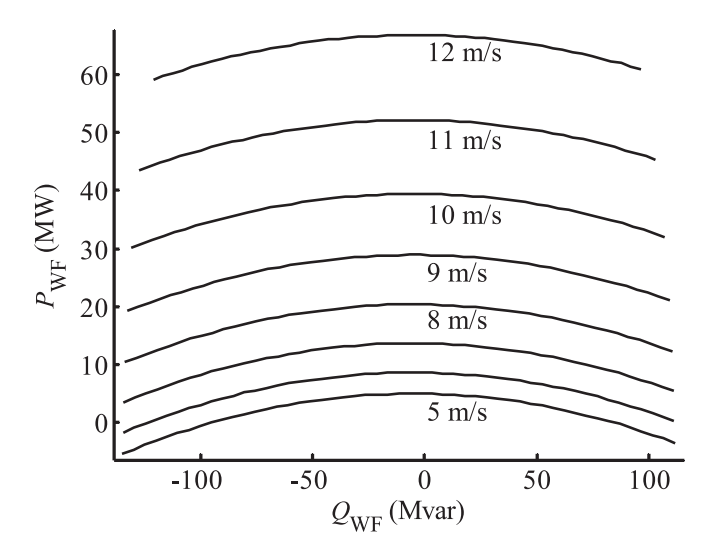


Fig. 19. Relation of P_{WF} with Q_{WF} with different v_{w} .

Table 8
PO-dependence of wind farm with different wind speeds.

$v_{\rm w}$ (m/s)	P_{WF} (MW)	P_{WF} (MW)			ξ_2 (%)
	Point A	Point B	Point C		
5	-3.5337	-5.4647	4.9148	211.19	-54.65
6	0.1902	-1.7281	8.5639	120.18	1.01×10^{3}
7	5.3724	3.4652	13.6332	74.58	35.50
8	12.2475	10.3480	20.3375	49.12	15.51
9	21.0489	19.1540	28.8777	33.67	9.00
10	32.0096	30.1209	39.4358	23.62	5.90
11	45.3603	43.4897	52.1730	16.64	4.12
12	60.9999	59.1899	66.8456	11.45	2.97

 $V_{\rm PCC}$, and $P_{\rm WF}$ is more dependent on $Q_{\rm WF}$. With lower $v_{\rm w}$, $P_{\rm WF}$ is smaller and more dependent on $Q_{\rm WF}$.

The proposed reactive power limit model of wind farm may be applied to the system-side analysis, e.g. power flow or power dispatch, to fully utilize the reactive power, estimate the impact of the reactive power on the active power, and enhance the dispatchability of wind farm for the system purpose. It may also be applied to other power stations with many small distributed generators.

Author Statement

The paper is the original work of the author. It does not copy or unsuitably cite any literature.

The paper does not copy or unsuitably cite any other literature. It is not published or under consideration by any other journal.

CRediT authorship contribution statement

Shenghu Li: Writing – review & editing, Writing – original draft, Validation, Software, Methodology, Investigation, Data curation, Conceptualization.

Declaration of competing interest

The authors declare that they have no known competing financial interests or personal relationships that could have appeared to influence the work reported in this paper.

Data availability

Data will be made available on request.

References

- Li S, Chen D, Qi N, Xia W. Active power reserve capacity range of DFIG based on the lower limit of steady-state active power of DFIG and small-disturbance stability sensitivity of power system. Southern Power Syst Technol 2023;17(8):1–10.
- [2] Wang Z, Wang Y, Davari M, Blaabjerg F. An effective PQ-decoupling control scheme using adaptive dynamic programming approach to reducing oscillations of virtual synchronous generators for grid connection with different impedance types. IEEE Trans Indus Electron 2024;71(4):3763–75.
- [3] Li S, Qi N. Triple-branch structure design and parameter optimization for supplementary damping controller of DFIG to suppress angular oscillation and reduce phase-locking error of PLL. Int. J. Electr. Power Energy Syst. 2024;162: 110327
- [4] Hu Q, Ji F, Ma F, Zhang Y, Fu L. Matching analysis of LVRT grid code and injection current dependent voltage response of WTC connected to high impedance ac grid. IEEE Trans. Energy Convers. 2022;37(3):2236–9.
- [5] Su X, Fang L, Yang J, Shahnia F, Fu Y, Dong ZY. Spatial-temporal coordinated volt/var control for active distribution systems. IEEE Trans. Power Syst. 2024;39(6): 7077–88
- [6] Li S. Sensitivity-based expression of the voltage-power characteristic (VPC) of the wind farm from the VPCs of the DFIGs and the collector. IEEE Trans. Power Syst. 2024;39(1):2143–53.
- [7] Pan C, Shao C, Hu B, Xie K, Li C, Ding J. Modeling the reserve capacity of wind power and the inherent decision-dependent uncertainty in the power system economic dispatch. IEEE Trans. Power Syst. 2023;38(5):4404–17.
- [8] Davoodi E, Capitanescu F. Wehenkel l.a methodology to evaluate reactive power reserves scarcity during the energy transition. IEEE Trans. Power Syst. 2023;38(5): 4355–68.
- [9] Xu S, Wu W, Yang Y, Lin C, Liu Y. Chance-constrained joint dispatch of generation and wind curtailment-load shedding schemes with large-scale wind power integration. IEEE Trans Sustain Energy 2023;14(4):2220–33.
- [10] Lu B, Li S, Das DS, Gao Y, Wang J, Baggu M. Dynamic P-Q capability and abnormal operation analysis of a wind turbine with doubly fed induction generator. IEEE J. Emerging Sel. Top. Power Electron. 2022;10(4):4854–64.
- [11] Zhang B, Hou P, Hu W, Soltani M, Chen C, Chen Z. A reactive power dispatch strategy with loss minimization for a DFIG-based wind farm. IEEE Trans. Power Syst. 2016;7(3):914–23.
- [12] Cui S, Yan X, Li R. Experimental research on improving the dynamic reactive power coordinated control capability of doubly-fed induction wind turbine. Power Syst Prot Control 2022;50(8):117–29.
- [13] Ghosh S, Isbeih YJ, Bhattarai R, Moursi MSE, El-Saadany EF, Kamalasadan S. A dynamic coordination control architecture for reactive power capability enhancement of the DFIG-based wind power generation. IEEE Trans. Power Syst. 2020;35(4):3051-64.
- [14] Lund T, Sorensen P, Eek J. Reactive power capability of a wind turbine with doubly fed induction generator. Wind Energy 2007;10:379–94.
- [15] Engelhardt S, Erlich I, Feltes C, Kretschmann J, Shewarega F. Reactive power capability of wind turbines based on doubly fed induction generators. IEEE Trans. Energy Convers. 2011;26(1):364–72.
- [16] Ouyang J, Tang T, Yao J, Li M. Active voltage control for DFIG-based wind farm integrated power system by coordinating active and reactive powers under wind speed variations. IEEE Trans. Energy Convers. 2019;34(3):1504–11.
- [17] Pulgar-Painemal H. Enforcement of current limits in DFIG-based wind turbine dynamic models through capability curve. IEEE Trans Sustain Energy 2019;10(1): 318–20.

- [18] Rong F, Li P, Zhou S. Coordinated optimal control with loss minimization for active and reactive power of doubly fed induction generator-based wind farm. Trans China Electrotech Soc 2020;35(3):520–9.
- [19] Dong Z, Li Z, Du L, Liu Y, Ding Z. Coordination strategy of large-scale DFIG-based wind farm for voltage support with high converter capacity utilization. IEEE Trans Sustain Energy 2021;12(2):1416–25.
- [20] Li S. Operation region of doubly-fed induction generators based on rotor slip under MPPT control and power dispatch. Electr. Power Compon. Syst. 2014;42(8): 808–17
- [21] Konopinski RJ, Vijayan P, Ajjarapu V. Extended reactive capability of DFIG wind parks for enhanced system performance. IEEE Trans. Power Syst. 2009;24(3):
- [22] Wang Y, Liao Y, Song Y, Zeng Q, Zheng Z. Distributed optimal control strategy of reactive power and voltage in wind farm. High Volt Eng 2022;48(12):5047–56.
- [23] Hoseinzadeh B, Blaabjerg F. A novel control technique for on-load tap changer to enlarge the reactive power capability of wind power plants. IET Gener. Transm. Distrib. 2022;16(14):2928–38.
- [24] Aghatehrani R, Kavasseri R. Reactive power management of a DFIG wind system in micro grids based on voltage sensitivity analysis. IEEE Trans Sustain Energy 2011;2 (4):451–8
- [25] Liu C, Zhang Z, Lai Q. Fast-tracking optimization of reactive power for wind farm considering short-term fluctuations of wind generations. Proc. CSEE 2023;43(15): 5850.63

- [26] Sujod M, Erlich I, Engelhardt S. Improving the reactive power capability of the DFIG-based wind turbine during operation around the synchronous speed. IEEE Trans. Energy Convers. 2013;28(3):736–45.
- [27] Li S. Power flow modeling considering detailed constraints of the DFIGs and collector networks based on 3-layer BFS and convergence improvement. Int. J. Electr. Power Energy Syst. 2023;147):1–13.
- [28] Fu Y, Liu Y, Huang L, Ying F, Li F. Collection system topology for deep-sea offshore wind farms considering wind characteristics. IEEE Trans. Energy Convers. 2022;37 (1):631–42.
- [29] Li S, Li L, Ding Z. Optimization method to the location and capacity of backup cables in wind farm with doubly-fed induction generator. Power Sys Technol 2024; 48(3):1125–32.
- [30] Guo Z, Wei W, Shahidehpour M, Chen L, Mei S. Two-timescale dynamic energy and reserve dispatch with wind power and energy storage. IEEE Trans Sustain Energy 2023;14(1):490–503.
- [31] Peng H, Huang S, Wei J, Wei C, Wu Q, Shen F, et al. Two-stage decentralized optimal voltage control in wind farms with hybrid ESSs. IEEE Trans. Power Syst. 2024;39(5):6552–65.
- [32] Li S, Xia W. Static voltage stability considering reactive power limit of salient synchronous generator and active power loss of exciter. Int. J. Electr. Power Energy Syst. 2024;159:110006.